BEM simulation of transient fluid flow phenomena

J. Ravnik & L. Škerget
University of Maribor, Faculty of Mechanical Engineering, Slovenia

Abstract

In this paper a Boundary Element Method based numerical algorithm is presented for the simulation of three-dimensional unsteady fluid flow and heat transfer. Four different time discretization techniques are considered and compared on a model unsteady heat diffusion problem. Analytical solution of the problem is used to designate the three point second-order finite different approximation of the accumulation term of the transport equations as the most accurate. This choice is incorporated into the flow solver and the developed algorithm is used to simulate Rayleigh–Bénard convection. Oscillatory and chaotic behaviour of the flow field and heat transfer are observed. Temperature slices and velocity vectors are presented. Heat flux is presented in terms of the Nusselt number.
Keywords: Boundary Element Method, Rayleigh–Bénard convection, velocity-vorticity formulation, time discretization.

1 Introduction

The Boundary Element Method (BEM) is a numerical technique that has been successfully applied for the solution of a wide variety of engineering problems and natural phenomena. In this paper we are focused on unsteady natural convection phenomena. A transient simulation is required, which must be able to capture the oscillatory and chaotic nature of the flow problem.

The paper presents a BEM based laminar viscous flow solver and focuses on the time discretization. Three implicit finite difference approximations and an explicit approximation of the accumulation term of the transport equations are compared against an analytical solution of a model problem. The three point second order finite difference approximation is then incorporated into the flow solver and used to obtain an unsteady solution of the Rayleigh–Bénard convection problem.

WIT Transactions on Modelling and Simulation, Vol 52, © 2011 WIT Press
www.witpress.com, ISSN 1743-355X (on-line)
doi:10.2495/BE110051

2 Governing equations

We consider laminar viscous fluid flow coupled with heat transfer in three-dimensional setting. The fluid properties are assumed constant. Buoyancy is modelled within the Boussinesq approximation, where density variation with temperature is considered only in the momentum source term. The non-dimensional velocity-vorticity formulation of Navier–Stokes equations for simulation of laminar viscous fluid flow coupled with heat transfer consists of the kinematics equation, the vorticity transport equation and the energy equation:

$$\nabla^2 \vec{v} + \vec{\nabla} \times \vec{\omega} = 0, \tag{1}$$

$$\frac{\partial \vec{\omega}}{\partial t} + (\vec{v} \cdot \vec{\nabla})\vec{\omega} = (\vec{\omega} \cdot \vec{\nabla})\vec{v} + Pr\nabla^2 \vec{\omega} - PrRa\vec{\nabla} \times T\vec{g}, \tag{2}$$

$$\frac{\partial T}{\partial t} + (\vec{v} \cdot \vec{\nabla})T = \nabla^2 T. \tag{3}$$

Here, the velocity field is denoted by $\vec{v}$, the vorticity by $\vec{\omega}$ and temperature by T. The flow and heat transfer of a fluid is defined by specifying the Rayleigh Ra and Prandtl Pr number values. They are defined as

$$Pr = \frac{\nu \rho c_p}{\lambda}, \tag{4}$$

where ν is the kinematic viscosity of the fluid, ρ is the density, c_p thermal capacity and λ heat conductivity. The Rayleigh number is defined by

$$Ra = Pr\frac{g\beta \Delta T \mathcal{L}^2}{\nu^2}, \tag{5}$$

where β is thermal expansion coefficient, $g = 9.81 m/s^2$, ΔT is the characteristic temperature difference and $\mathcal{L}$ is the characteristic length scale of the system.

3 Time discretization

The main aim of this work was to study transient phenomena. We chose Rayleigh–Bénard convection for the test case. When fluid is heated from below, it very soon becomes unsteady and exhibits a wide range of time dependent phenomena. In order to estimate the accuracy of time discretization, we compared three implicit approximations of the time derivative and an explicit Runge–Kutta scheme.

In order to be able to compare the accuracy of different schemes, we chose the following heat transfer example. Consider a thermally isolated thin thread of length π. At the beginning of the simulation the thread has a certain temperature profile. As time passes the thread cools by emitting heat flux through both ends. Since the thread is isolated, there is no heat flux through the casing, and the problem can be treated as one-dimensional. The material properties of the thread are such, that the following equation is valid

$$\frac{\partial T}{\partial t} = \frac{\partial^2 T}{\partial x^2}. \tag{6}$$

The equation includes only accumulation and diffusion terms and is a simplification of (3), where the advection term is also present. At $t = 0$ a triangular temperature profile is applied to the thread.

$$T(x,0) = \begin{cases} 2\frac{x}{\pi}, & x \in (0, \pi/2); \\ 2\frac{\pi - x}{\pi}, & x \in (\pi/2, \pi). \end{cases} \tag{7}$$

A Dirichlet boundary condition is applied on both sides, i.e. $T(x = 0) = 0$ and $T(x = \pi) = 0$. Figure 1 shows the sketch of the problem along with boundary and initial conditions. The analytical solution of the problem gives temperature dependence of x and time. It is (Weisstein [1]):

$$T(x,t) = \frac{2}{\pi}\sum_{n=0}^{\infty}\left\{2\int_0^{\pi/2}\sin(nx)\frac{x}{\pi}dx + 2\int_{\pi/2}^{\pi}\sin(nx)x\frac{\pi - x}{\pi}dx\right\}\cdot$$
$$\cdot\sin(nx)e^{-n^2 t}. \tag{8}$$

The time dependent diffusion equation (6) is discretizised using subdomain BEM technique. Denoting the subdomain with Ω and its boundary with Γ, the following integral equation is obtained

$$c(\vec{\xi})T(\vec{\xi}) + \int_\Gamma T\vec{\nabla}u^* \cdot \vec{n}d\Gamma = \int_\Gamma u^* q_T d\Gamma + \int_\Omega f(T, T', T'', \Delta t)u^* d\Omega, \tag{9}$$

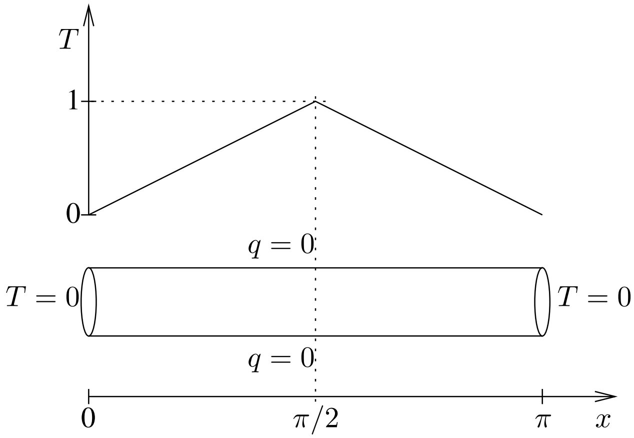

Figure 1: Boundary and initial conditions for time depended diffusion test case.

where $\vec{\xi}$ is the source or collocation point, $\vec{n}$ is a vector normal to the boundary, pointing out of the domain and $u^\star$ is the fundamental solution for the diffusion operator: $u^\star = 1/4\pi|\vec{\xi} - \vec{r}|$. q_T is the heat flux defined by $q_T = \vec{\nabla}T \cdot \vec{n}$. $c(\vec{\xi})$ is the geometric factor defined as $c(\vec{\xi}) = \alpha/4\pi$, where α is the inner angle with origin in $\vec{\xi}$.

Function $f(T, T', T'', \Delta t)$ denotes the discretization of the time derivative;

$$\frac{\partial T}{\partial t} = f(T, T', T'', \Delta t). \tag{10}$$

The discrete version of the partial time derivative may depend on the time step Δt, temperature in the next time step T, temperature in the current time step T' and temperature in the previous time step T''.

Firstly, we consider first order *backward Euler* approximation of the time derivative defined by

$$\frac{\partial T}{\partial t} \approx \frac{T - T'}{\Delta t}, \tag{11}$$

secondly the second order *trapezoid* scheme

$$\frac{\partial T}{\partial t} \approx \frac{1}{2}\frac{T - T'}{\Delta t} + \frac{1}{2}\frac{T' - T''}{\Delta t} = \frac{1}{2}\frac{T - T''}{\Delta t}, \tag{12}$$

and thirdly a *three point* second order scheme defined by

$$\frac{\partial T}{\partial t} \approx \frac{3T - 4T' + T''}{2\Delta t}. \tag{13}$$

The three finite difference approximation of the time derivative are all implicit, i.e. they include a temperature value that must be calculated. This contribution is added to the system matrix when the system of linear equations is formed.

Furthermore, we consider an explicit Runge–Kutta type scheme. Since the scheme is explicit, we estimate the partial time derivate in the present time step and use its value to get the function value at the next time step. Fourth order scheme was used, given by the following algorithm

1. $T^{(1)} = T' + \frac{1}{4}\Delta t \left[a\frac{\partial^2 T}{\partial x^2}\right]'$
2. $T^{(2)} = T' + \frac{1}{3}\Delta t \left[a\frac{\partial^2 T}{\partial x^2}\right]^{(1)}$
3. $T^{(3)} = T' + \frac{1}{2}\Delta t \left[a\frac{\partial^2 T}{\partial x^2}\right]^{(2)}$
4. $T = T' + \Delta t \left[a\frac{\partial^2 T}{\partial x^2}\right]^{(3)}$

Time step size for the Runge–Kutta scheme is limited by the Courant–Friedrichs–Lewy stability condition:

$$\Delta t \leq \frac{\mu \Delta x}{\delta}, \tag{14}$$

where $\mu < 1$ is the Courant–Friedrichs–Lewy number, δx the mesh size and δ a characteristic velocity.

Table 1: Comparison of temperature in the middle of the domain; $T(\pi/2, 1)$.

Δt	No. of time steps	Euler	Trapezoid	3 point	Runge–Kutta
0.1	10	0.3127	0.3263	0.2995	
0.01	100	0.2997	0.3012	0.2982	
0.001	1000	0.2984	0.2985	0.2982	
0.0001	10^4				0.2982
Analytical		0.2982	0.2982	0.2982	0.2982

The four time discretization schemes using different time steps were compared against the analytical solution. A time of $t = 1$ was chosen to compare temperature profiles. A mesh of 100 equidistant quadratic elements having 201 nodes in x direction was used to solve the problem. Table 1 provides temperature values in the middle of the domain (at $x = \pi/2$) for different time steps along with the analytical solution. Figures 2 and 3 show the comparison of temperature profiles at $t = 1$.

The results clearly show, that the three point scheme (13) gives the most accurate results. The explicit scheme also yields very accurate results, but unfortunately requires a very large number of time steps, due to the Courant-Friedrichs-Lewy (14) stability condition.

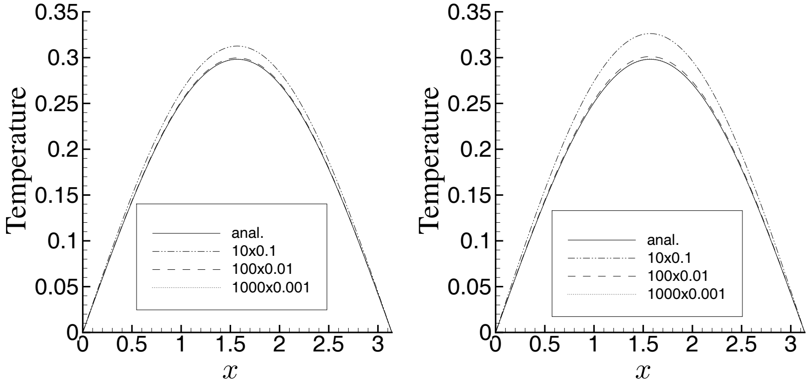

Figure 2: Time dependent solution of diffusion equation. Comparison of analytic and simulated temperature profiles for different time step lengths. Left backward Euler scheme and right trapezoid scheme.

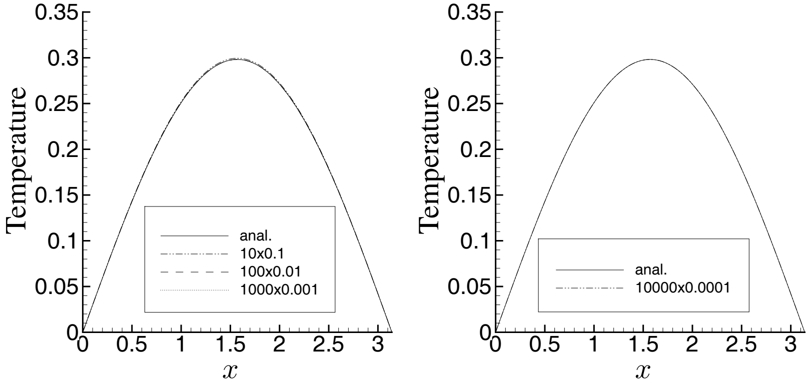

Figure 3: Time dependent solution of diffusion equation. Comparison of analytic and simulated temperature profiles for different time step lengths. Left three point scheme and right Runge Kutta scheme.

4 Numerical method

With the choice of the time discretization established, we proceeded to rewrite the governing equations (1)–(3) in integral form. Three-dimensional solver capable of steady simulating flow and heat transfer by solving velocity-vorticity formulation of Navier–Stokes equations by a combination of single and sub-domain BEM was developed by Ravnik et al. [2, 3]. Integral equations were written in the same manner with an addition of the discretization of the accumulation term.

The kinematics equation is

$$c(\vec{\xi})\vec{n}(\vec{\xi}) \times \vec{v}(\vec{\xi}) + \vec{n}(\vec{\xi}) \times \int_\Gamma \vec{v}\vec{\nabla}u^\star \cdot \vec{n}d\Gamma$$

$$= \vec{n}(\vec{\xi}) \times \int_\Gamma \vec{v} \times (\vec{n} \times \vec{\nabla})u^\star d\Gamma + \vec{n}(\vec{\xi}) \times \int_\Omega (\vec{\omega} \times \vec{\nabla}u^\star)d\Omega. \qquad (15)$$

In order to write a linear system of equations for the unknown boundary vorticity values, we set the source point into every boundary node of the whole computational domain. This yields a full system matrix where number of rows and columns is equal to number of boundary nodes. It is solved using a LU decomposition method.

The partial derivative with respect to time in the kinetics equations is approximated by second order three point finite difference scheme. The final forms of vorticity transport and energy equation are

$$c(\vec{\xi})\omega_j(\vec{\xi}) + \int_\Gamma \omega_j \vec{\nabla}u^* \cdot \vec{n}d\Gamma = \int_\Gamma u^* q_j d\Gamma +$$

$$+\frac{1}{Pr}\left(\int_\Gamma \vec{n} \cdot \{u^*(\vec{v}\omega_j - \vec{\omega}v_j)\}\, d\Gamma - \int_\Omega (\vec{v}\omega_j - \vec{\omega}v_j) \cdot \vec{\nabla}u^* d\Omega\right)$$

$$-Ra\left(\int_\Gamma (u^\star T\vec{g}\times\vec{n})_j d\Gamma + \int_\Omega (T\vec{\nabla}\times u^\star\vec{g})_j d\Omega\right)$$
$$+\frac{1}{Pr}\frac{1}{2\Delta t}\int_\Omega (3\omega_j - 4\omega_j' + \omega_j'')u^* d\Omega, \qquad (16)$$

$$c(\vec{\xi})T(\vec{\xi}) + \int_\Gamma T\vec{\nabla}u^*\cdot\vec{n}d\Gamma = \int_\Gamma u^* q_T d\Gamma + \int_\Gamma \vec{n}\cdot\{u^*(\vec{v}T)\}\,d\Gamma$$
$$-\int_\Omega (\vec{v}T)\cdot\vec{\nabla}u^* d\Omega + \frac{1}{2\Delta t}\int_\Omega (3T - 4T' + T'')u^* d\Omega, \qquad (17)$$

where ω_j is the j^{th} component of vorticity.

In the subdomain BEM method we make a mesh of the entire domain Ω and name each mesh element a subdomain. Equation (16) is written for each of the subdomains. In order to obtain a discrete version of (16) we use shape functions to interpolate field functions and flux across the boundary and inside of the subdomain. In this work we used hexahedral subdomains, which enable continuous quadratic interpolation of field functions. On each boundary element we interpolate the flux using discontinuous linear interpolation scheme. By using discontinuous interpolation we avoid flux definition problems in corners and edges. A function, e.g. temperature, is interpolated over a boundary elements as $T = \sum \varphi_i T_i$, inside each subdomain as $T = \sum \Phi_i T_i$, while flux is interpolated over boundary elements as $q = \sum \phi_i q_i$. The following integrals must be calculated:

$$[H] = \int_\Gamma \varphi_i \vec{\nabla}u^\star\cdot\vec{n}d\Gamma, \quad [G] = \int_\Gamma \phi_i u^\star d\Gamma, \quad [\vec{A}] = \int_\Gamma \varphi_i \vec{n}u^\star d\Gamma, \qquad (18)$$

$$[B] = \int_\Omega \Phi_i u^\star d\Omega, \qquad [\vec{D}] = \int_\Omega \Phi_i \vec{\nabla}u^\star d\Omega. \qquad (19)$$

The square brackets denote integral matrices. In order to calculate the integrals, a Gaussian quadrature algorithm is used. Calculation of the free coefficient $c(\vec{\xi})$ is preformed indirectly considering rigid body movement problem solution. The calculated $c(\vec{\xi})$ are added to the diagonal terms of the $[H]$ matrix.

The source point is set to all function and flux node in each subdomain. Since neighbouring subdomains share nodes, the resulting systems of linear equations are over-determined. After taking into account the boundary conditions, we solve them using a least squares solver (Paige and Saunders [4]). All integrals depend only on the shape of subdomains and as such may be calculated only once, prior to the start of the nonlinear iterative process.

The algorithm used to solve the set of governing equations (1)–(3) is devised as follows. Either Dirichlet or Neumann type boundary conditions for velocity and temperature must be known. In this paper we use the no-slip boundary condition on all solid walls and prescribe temperature or temperature flux. Boundary conditions for vorticity are unknown and are calculated as a part of the algorithm. The following steps are performed.

Within each time step do the following. Firstly, calculate vorticity values on the boundary by single domain BEM from the kinematics equation (1). Secondly calculate velocity values by sub-domain BEM from the kinematics equation (1). Next calculate temperature values by sub-domain BEM from the energy equation (3). Next calculate vorticity values in the domain by sub-domain BEM from the vorticity transport equation (2). Finally check convergence. If all flow fields converged to 10^{-6} stop, else go to 2. When a time step has converged, advance the flow fields for one time step, i.e. use $T'' = T'$ and $T' = T$ and repeat the procedure for the next time step. Convergence was accelerated using an algorithm for adaptive setting of solver accuracy, developed by Ravnik et al. [5].

5 Rayleigh–Bénard convection

In order to test the capability of the method to simulate unsteady flows, we simulated the Rayleigh–Bénard convection (Solomon and Gollub [6], Shan [7]). The domain was a cubic cavity, where the bottom wall was heated to a constant temperature and the top wall cooled to an also constant but lower temperature. The temperature difference between the walls defines the Rayleigh number for this case. The vertical walls of the cavity are insulated. No-slip velocity boundary conditions are applied on all walls. Boundary conditions are sketched in Figure 4.

Meshes of 16^3 elements having in total 33^3 nodes and mesh of 20^3 elements with 41^3 nodes were used. Simulation were run with air ($Pr = 0.71$) as the working fluid and Rayleigh number values of $Ra = 10^5$ and $Ra = 10^6$. Nondimensional time step of $\Delta t = 0.001$ was used. Preliminary results on the coarse mesh proved significantly different from the results obtained on the fine mesh, thus all simulations were preformed on the fine mesh.

In both cases ($Ra = 10^5$ and $Ra = 10^6$) the flow field was unsteady exhibiting a variety of structures in the domain. Figures 5 and 6 show two times instants, giving

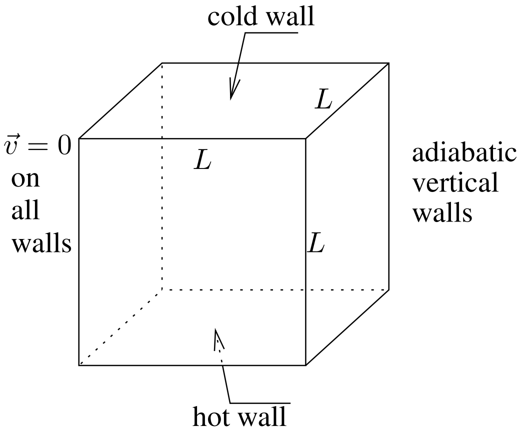

Figure 4: Boundary conditions for the simulation of Rayleigh–Bénard convection.

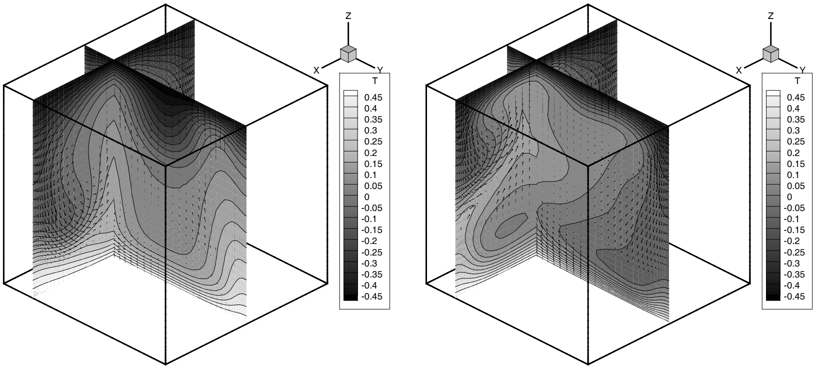

Figure 5: Two slices showing the temperature field and velocity vectors at $Ra = 10^5$. There are 199 time steps between the left and right figure.

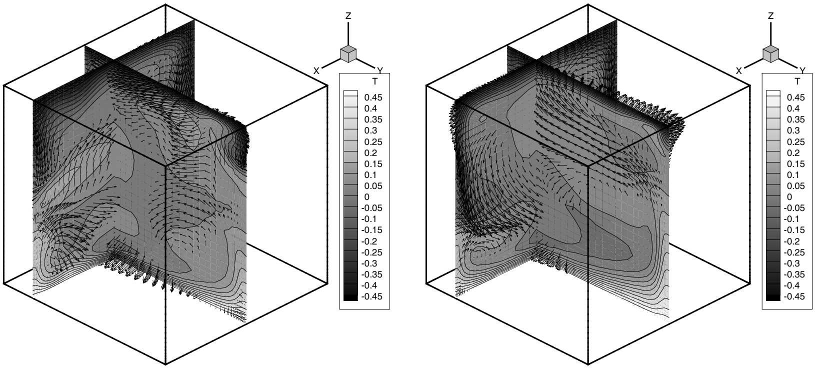

Figure 6: Two slices showing the temperature field and velocity vectors at $Ra = 10^6$. There are 80 time steps between the left and right figure.

an impression of the changing temperature and velocity fields. For $Ra = 10^5$ these changes are slow compared to the rapid and unpredictable flow and temperature pattern at $Ra = 10^6$. After a long time, flow at $Ra = 10^5$ stabilised and reached steady state. The final, steady flow field is shown in Figure 7.

During the simulation heat transfer through the top and bottom walls was measured in terms of Nusselt number value. Usually, the heat flux $\dot{Q}$ is expressed in terms of fluid thermal conductivity, characteristic flow scale and a non-dimensional Nusselt number, i.e. $\dot{Q} = \lambda \mathcal{L} \Delta T \cdot Nu$. The Nusselt number, Nu, is defined as the integral of the temperature flux through a wall:

$$Nu = \int_\Gamma \vec{\nabla} T \cdot \vec{n} d\Gamma, \tag{20}$$

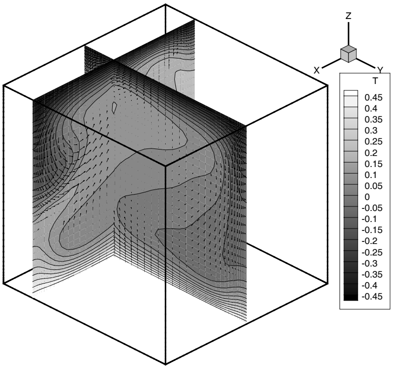

Figure 7: Two slices showing the temperature field and velocity vectors at $Ra = 10^5$ for the final steady flow configuration.

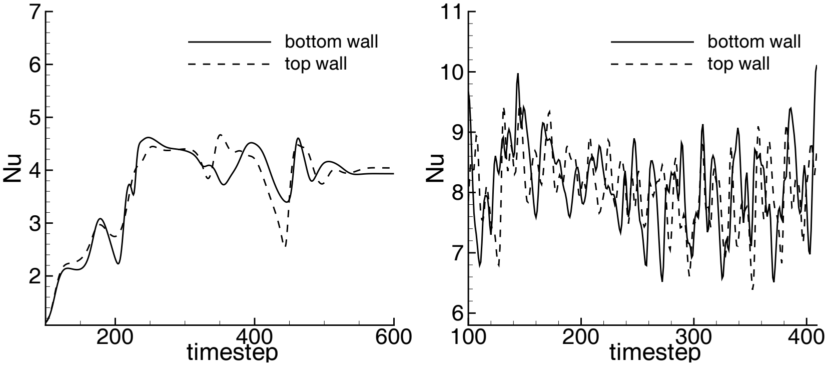

Figure 8: Development of heat flow through the top and bottom walls in the Rayleigh–Bénard convection case; left $Ra = 10^5$, right $Ra = 10^6$.

where Γ is the surface through which we calculate the heat flux and $\vec{n}$ is a unit normal to this surface. We also study local variation of heat flux using the local Nusselt number defined as $Nu_l(x, y, z) = \vec{\nabla} T \cdot \vec{n}$.

The development of heat flux through time is shown in Figure 8. In the $Ra = 10^5$ case the heat flux slowly varies in time and reaches steady state after about 600 time steps. At steady state, heat fluxes through top and bottom walls are equal, reaching $Nu = 3.98$. In the $Ra = 10^6$ case steady state is not reached. The chaotic nature of the graphs indicates that the flow regime is past the oscillatory unsteady phase in a chaotic regime heading towards turbulence at higher Rayleigh number values.

Figure 9 shows heat flux variation through top and bottom walls for the $Ra = 10^5$ case. The heat flux is expressed using the local Nusselt number. Symmetric distribution of fluxes is observed. This is consistent with the fact that the flow

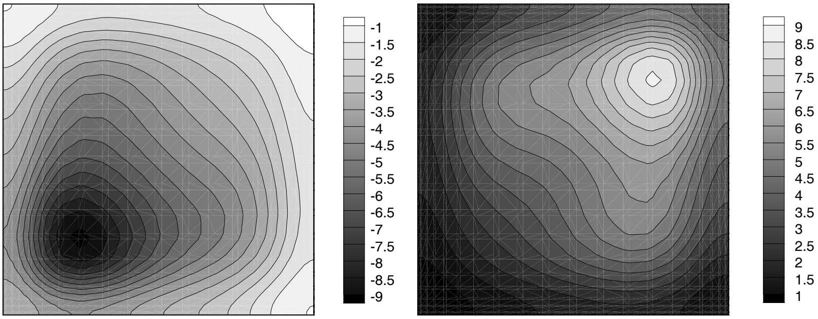

Figure 9: Heat flux (local Nusselt number) through the top (left) and bottom (right) walls at $Ra = 10^5$.

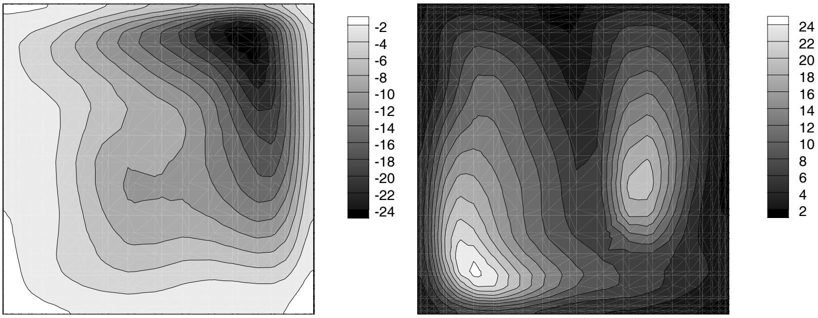

Figure 10: Heat flux (local Nusselt number) through the top (left) and bottom (right) walls at $Ra = 10^6$.

reached steady state and that the same amount of heat entering the domain through the bottom wall also exits through the top wall. Figure 10 presents the $Ra = 10^6$ case at some time during the simulation. Here steady state is not reached and the heat fluxes through the top an bottom wall are distinctly different.

6 Summary and outlook

We presented a boundary element based method for simulation of unsteady laminar viscous flows coupled with heat transfer. The method solves the velocity-vorticity formulation of Navier–Stokes equations using a combination of single domain BEM and subdomain BEM. A study of different approximations of time derivate of the governing equations showed that the second order three point finite difference approximation yields the most accurate results at a given time step size. The algorithm was successfully used for simulation Rayleigh–Bénard convection, showing a unsteady behaviour on the verge of chaos.

In this work a diffusion type fundamental solution was used to write the integral equation. In future, we plan to use the time dependent diffusion-advection type fundamental solution, with which the need for discretization of the accumulation term would be avoided. First successful attempts in this direction were done in 2D by Škerget et al. [8] using the parabolic diffusion fundamental solution.

References

[1] Weisstein, E.W., Heat conduction equation. *MathWorld–A Wolfram Web Resource*, 2005.

[2] Ravnik, J., Škerget, L. & Žunič, Z., Combined single domain and subdomain BEM for 3D laminar viscous flow. *Eng Anal Bound Elem*, **33**, pp. 420–424, 2009.

[3] Ravnik, J., Škerget, L. & Žunič, Z., Velocity-vorticity formulation for 3D natural convection in an inclined enclosure by BEM. *Int J Heat Mass Transfer*, **51**, pp. 4517–4527, 2008.

[4] Paige, C.C. & Saunders, M.A., LSQR: An algorithm for sparse linear equations and sparse least squares. *ACM Transactions on Mathematical Software*, **8**, pp. 43–71, 1982.

[5] Ravnik, J., Škerget, L. & Hriberšek, M., Analysis of three-dimensional natural convection of nanofluids by BEM. *Eng Anal Bound Elem*, **34**, pp. 1018–1030, 2010.

[6] Solomon, T. & Gollub, J., Chaotic particle transport in time-dependent Rayleigh–Benard convection. *Physical Review A*, **38(12)**, pp. 6280–6286, 1988.

[7] Shan, X., Simulation of Rayleigh–Benard convection using a lattice Boltzmann method. *Physical Review E*, **55(3)**, pp. 2780–2788, 1997.

[8] Škerget, L., Hriberšek, M. & Žunič, Z., Natural convection flows in complex cavities by BEM. *Int J Num Meth Heat & Fluid Fl*, **13**, pp. 720–735, 2003.